JOURNAL OF SYNCHROTRON RADIATION
ISSN 1600-5775

Miniature diamond anvils for X-ray Raman scattering spectroscopy experiments at high pressure

Sylvain Petitgirard,[a]* Georg Spiekermann,[b] Christopher Weis,[c] Christoph Sahle,[d] Christian Sternemann[c] and Max Wilke[b]

[a]University of Bayreuth, Bayerisches Geoinstitut, Universitätsstrasse 30, Bayreuth, 95447, Germany, [b]Universität Potsdam, Potsdam, Germany, [c]Fakultät Physik / DELTA, Technische Universität Dortmund, D-44221 Dortmund, Germany, and [d]European Synchrotron Radiation Facility, Grenoble, France. *Correspondence e-mail: sylvain.petitgirard@uni-bayreuth.de

Received 13 September 2016
Accepted 24 October 2016

Edited by S. M. Heald, Argonne National Laboratory, USA

Keywords: X-ray Raman scattering; high pressure; miniature diamond anvils; SiO_2 glass.

X-ray Raman scattering (XRS) spectroscopy is an inelastic scattering method that uses hard X-rays of the order of 10 keV to measure energy-loss spectra at absorption edges of light elements (Si, Mg, O *etc.*), with an energy resolution below 1 eV. The high-energy X-rays employed with this technique can penetrate thick or dense sample containers such as the diamond anvils employed in high-pressure cells. Here, we describe the use of custom-made conical miniature diamond anvils of less than 500 µm thickness which allow pressure generation of up to 70 GPa. This set-up overcomes the limitations of the XRS technique in very high-pressure measurements (>10 GPa) by drastically improving the signal-to-noise ratio. The conical shape of the base of the diamonds gives a 70° opening angle, enabling measurements in both low- and high-angle scattering geometry. This reduction of the diamond thickness to one-third of the classical diamond anvils considerably lowers the attenuation of the incoming and the scattered beams and thus enhances the signal-to-noise ratio significantly. A further improvement of the signal-to-background ratio is obtained by a recess of ~20 µm that is milled in the culet of the miniature anvils. This recess increases the sample scattering volume by a factor of three at a pressure of 60 GPa. Examples of X-ray Raman spectra collected at the O *K*-edge and Si *L*-edge in SiO_2 glass at high pressures up to 47 GPa demonstrate the significant improvement and potential for spectroscopic studies of low-*Z* elements at high pressure.

1. Introduction

SiO_2 glass has attracted a lot of attention over the past decades (Mozzi & Warren, 1969; Woodcock *et al.*, 1976; Hemley *et al.*, 1986) because it often serves as a reference model to explain, or compare, the behavior of other amorphous silicate compounds (Sanchez-Valle & Bass, 2010; Murakami & Bass, 2011; Sakamaki *et al.*, 2014) and melts at high pressure (Sanloup *et al.*, 2013; Millot *et al.*, 2015). At the pressure conditions of the Earth's lower mantle, glasses and melts become as dense as their crystalline counterparts (Sato & Funamori, 2008; Petitgirard *et al.*, 2015), which could be linked to a coordination increase of silicon, from initially four oxygen neighbors to five, six and maybe more neighboring oxygen atoms at high pressure, as proposed by molecular dynamics simulations (Stixrude & Karki, 2005; Wu *et al.*, 2012; Ghosh *et al.*, 2014). However, such changes and compaction mechanisms remain debated because of a lack of direct experimental information on the coordination of such elements in glasses and melts at high pressure. For instance, the fourfold to sixfold

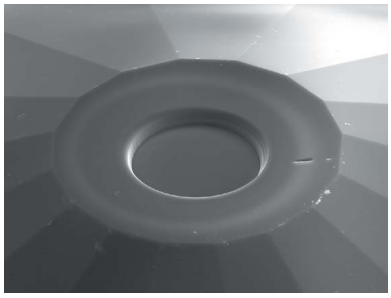

transformation in SiO_2 has been proposed to happen very rapidly with pressure to reach sixfold coordination at 40 GPa (Sato & Funamori, 2008), whereas another report suggests that fourfold coordination could be preserved up to 20 GPa and that sixfold coordination might be completed above 50–60 GPa (Benmore *et al.*, 2010). At extreme pressure conditions, close to the core-mantle boundary at 135 GPa, SiO_2 (Murakami & Bass, 2010) and $MgSiO_3$ (Murakami & Bass, 2011) may experience a further densification that could be attributed to an increase of coordination higher than sixfold, but these changes have not been confirmed elsewhere. To clarify such issues, it is important to measure directly the electronic environment associated with coordination changes in SiO_2 using near-edge X-ray absorption spectroscopy at the Si *L*-edge and O *K*-edge. However, these absorption edges lie at approximately 100 eV and 540 eV, respectively. Therefore, both edges are inaccessible for soft X-ray absorption and electron energy-loss spectroscopy when working at high pressures with diamond anvils. This problem can be circumvented by using X-ray Raman scattering (XRS) spectroscopy, which is a non-resonant inelastic X-ray scattering technique (Bergmann *et al.*, 2002; Krisch & Sette, 2002; Wernet *et al.*, 2002; Sternemann *et al.*, 2005; Fister *et al.*, 2008; Huotari *et al.*, 2010; Nilsson *et al.*, 2010); a comprehensive review on XRS is given by Schülke (2007). XRS spectroscopy allows *K*-edges of light elements (Li, C, O, *etc*.) as well as *L*-edges of medium-*Z* elements (Mg, Al, Si *etc*.) to be measured using hard X-rays of between about 6 and 20 keV (Schülke, 2007). This method has been applied to a variety of high-pressure studies (Rueff & Shukla, 2010; Lee *et al.*, 2014; Sternemann & Wilke, 2016) but often the low signal-to-noise ratio complicated a detailed interpretation of the data. In some experimental cases, the X-ray Raman cross section is approximately proportional to the absorption cross section (Mizuno & Ohmura, 1967), and the optimum thickness for scattering in transmission geometry, which balances the number of scatters with the absorption, is achieved when the sample thickness is equal to the value $1/\mu$. where μ is the linear X-ray absorption coefficient of the sample. This will vary with the composition and density of the sample as well as the incident photon energy. XRS has been employed to measure the oxygen *K*-edge in $MgSiO_3$ (Lee *et al.*, 2008; Hiraoka *et al.*, 2016) and SiO_2 (Lin *et al.*, 2007) glasses through beryllium gaskets, and also XRS spectra for both compositions have been calculated on the basis of MD simulations (Wu *et al.*, 2012; Yi & Lee, 2016). For both systems, the spectral changes with pressure are attributed to the formation of oxygen clusters and, indirectly, to the coordination change of silicon. In order to fully understand the structural changes it is of prime importance to measure directly the electronic structure of the cations of such glasses, Si and Mg. However, the Be *K*-edge is very close in energy to the silicon *L*-edge. Therefore, the use of Be gaskets significantly complicates probing the local environment of Si in very much detail. Only one XRS experiment has attempted to probe the silicon *L*-edge in SiO_2 glass through the diamond anvils (Fukui *et al.*, 2008), but the report is inconclusive because of a poor energy resolution and a very weak signal-to-background ratio.

To overcome the strong attenuation of both the incoming and the scattered X-ray beams by the diamonds, we have developed miniature diamond anvils of less than 500 µm thickness that can sustain pressure of at least 70 GPa based on the standard Boehler–Almax design (Boehler & De Hantsetters, 2004). We improved the signal-to-background ratio further by increasing the sample volume by a factor of three at high pressure by milling recesses in both diamond culets. The design and test of the miniature anvils are presented in this paper, after a short introduction of the beamline set-up and the procedure of data extraction. Finally, XRS spectra on the oxygen *K*-edge and the silicon *L*-edge measured up to 47 GPa are discussed and compared with reference materials. They show a considerable improvement in data quality when using miniature diamond anvils for XRS experiments conducted around 10 keV with sub-eV resolution.

2. Beamline set-up, measurement geometry and data extraction

In this section we give a simple description of the experimental set-up and the parameters we used to measure the silicon *L*-edge and oxygen *K*-edge in SiO_2 at high pressure. A more detailed description of XRS and the potential of the technique can be found elsewhere (Sahle *et al.*, 2015), with references therein. The measurements were performed at the ID20 beamline (ESRF, France). The source is composed of four U26 undulators to maximize the incident flux. The working incident energy (E_0) of 9.7 keV is selected firstly by using a high-heat-load liquid-nitrogen-cooled Si(111) pre-monochromator with an energy resolution of $\Delta E/E = 1.1 \times 10^{-4}$. A consecutive Si(311) channel-cut post-monochromator further reduces the incident bandwidth to approximately 0.4 eV.

Worldwide, most XRS set-ups at synchrotron facilities are able to work with different incident X-ray energies of 6.4, 9.7, 12.9 keV or higher (Hiraoka *et al.*, 2013). When the spectrometer employs spherically bent Si analyzer crystals in Bragg geometry, the highest overall final energy resolution is obtained with the lowest incident energy. The highest energy resolution (0.3 eV) is obtained with an incident beam of 6.4 keV. However, it is not very suitable for a diamond-anvil cell (DAC) as most of the incident beam will be absorbed by the diamonds. On the other hand, at 12.9 keV incident energy, the energy resolution is about 1.5 eV, which is too low to resolve important pressure-induced changes in the shape of the silicon *L*-edge for instance. The incident energy of 9.7 keV is a good compromise, with an energy resolution of about 0.7 eV (for the described set-up) and an attenuation of the incident beam to about 40% in the path through a standard diamond of about 2 mm thickness.

The incident X-ray beam at ID20 can be focused down to ~10 µm × 20 µm (V × H) through a pair of Kirkpatrick–Baez mirrors (Fig. 1). The DAC is placed on a goniometer stage and enclosed in a vacuum chamber to limit air scattering.

The XRS spectrometer at ID20 is composed of six movable analyzer chambers, three in the vertical plane and three in the horizontal plane, each containing 12 Si(660) spherically curved

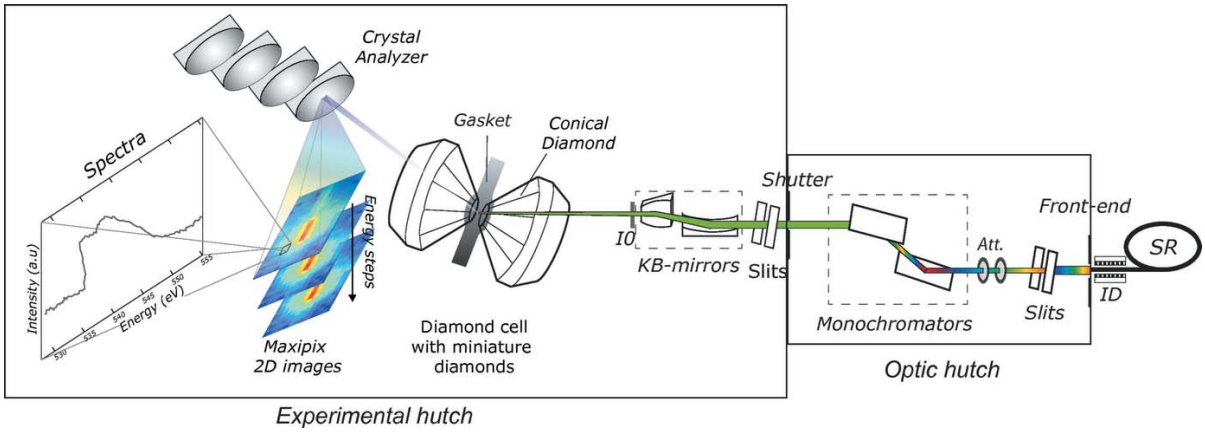

Figure 1
Measurement geometry and set-up description on ID20. Synchrotron radiation generates photons through the four-undulator insertion device (ID). The photon beam is shaped through slits and a specific wavelength is selected *via* two monochromators (a pre-monochromator and a channel-cut post-monochromator). The beam is focused down to 10 µm × 20 µm using two KB mirrors onto the sample in the DAC. Spherical crystal analyzers reflect the scattered signal from the sample and diamond. They are used as focusing monochromator enabling a sub-eV (0.7 eV) final resolution. The scattered image is collected on a two-dimensional Maxipix pixel detector, one for each row of the four crystal analyzers.

crystal analyzers, arranged in three rows of four crystals. The crystal analyzers act as a focusing monochromator enabling a sub-eV (0.7 eV) final resolution when working at 9.7 keV. The chambers can be placed in both the forward and the back-scattering geometry at a different angle with respect to the incoming beam, allowing probing the sample at different momentum transfer $|q|$ up to a maximum of 10 Å^{-1}.

The signal, reflected on the crystal analyzers, is collected on two-dimensional Maxipix pixel area detectors (Ponchut *et al.*, 2011), one for each analyzer chamber (Fig. 1). Two-dimensional images are collected at each energy step on all detectors. The images contain the scattering signal of the sample as well as the scattering of surrounding material (*i.e.* diamond anvils), and a pixel-by-pixel investigation is performed to find the one or two pixels that contain the signal from the sample. Once the right pixels are found, they can be summed-up for each energy step generating one near-edge spectrum for each analyzer crystal (Fig. 1). Spectra with similar momentum transfer $|q|$ can be averaged over further, resulting in the data shown here. A more detailed explanation of the theory of XRS, pixel-by-pixel data extraction and analysis of DAC-contained samples is given by Sahle *et al.* (2017).

In our experiment, both the forward and the backward scattering geometries were used in order to enhance the signal and reduce the collection time per pressure points. Using the large opening angle of the DACs, it is then possible to use at least 2 to 3 Si(660) analyser arrays of the XRS spectrometer installed at ID20, which gives a total of 24–36 out of 72 crystal analysers.

3. Miniature diamond anvils for XRS

We have developed thinner diamond anvils in order to reduce the attenuation of the incoming and the scattered X-ray beams. These thinner anvils maintain similar characteristics to the standard diamond anvils: (i) 60° conical support surface based on the Boehler–Almax (Boehler & De Hantsetters, 2004) design; (ii) 70° opening at the base of the diamond allowing for backscattering geometry, in order to access both high and low momentum transfer ($|q|$) and (iii) similar target pressure capabilities with similar culet sizes (relative to standard design anvils). All diamond anvils had similar Boehler–Almax conical designs and were manufactured by Almax-easylab©.

3.1. Presentation and test of mini-anvils

We have tested several designs with different thicknesses: 0.9 mm, 0.7 mm and 0.48 mm. All anvils had culet sizes of 250 µm or 200 µm in diameter. As illustrated in Fig. 2(*a*), the

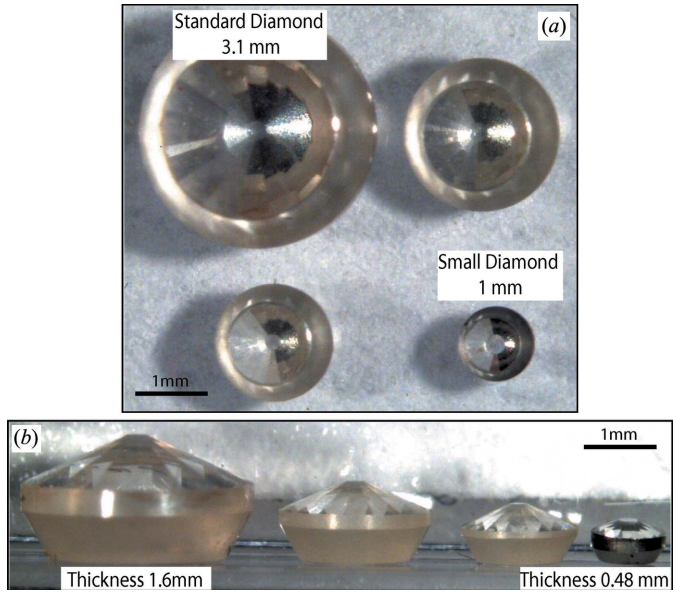

Figure 2
Photographs of different tested anvils. (*a*) Diamond anvils illustrating the change in diameter from standard design down to 1 mm diameter. (*b*) Diamond anvils illustrating the decrease in thickness from standard design to the smallest 0.48 mm miniature diamond anvil tested here.

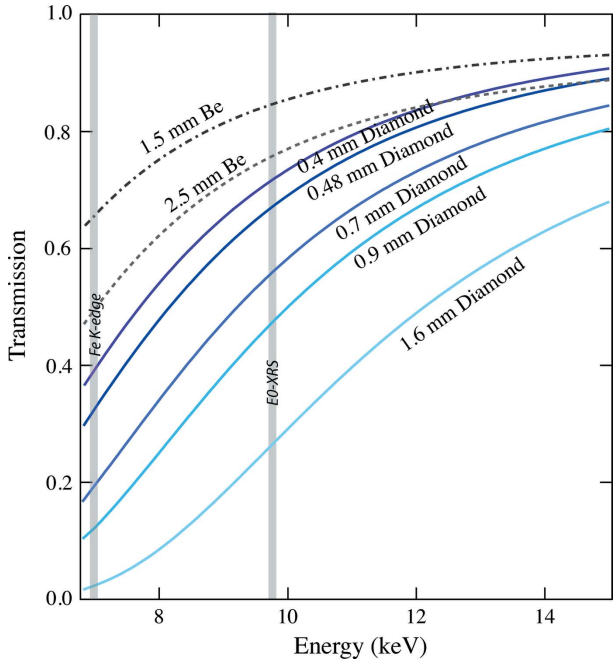

Figure 3
X-ray transmission calculated through various thicknesses of diamond (representative for one anvil) *versus* Be (thickness for half of a gasket) at different X-ray energies. Reported on the graph are the energy for the iron *K*-edge and the incident energy used for this XRS experiment $E_0 \simeq 9.7$ keV.

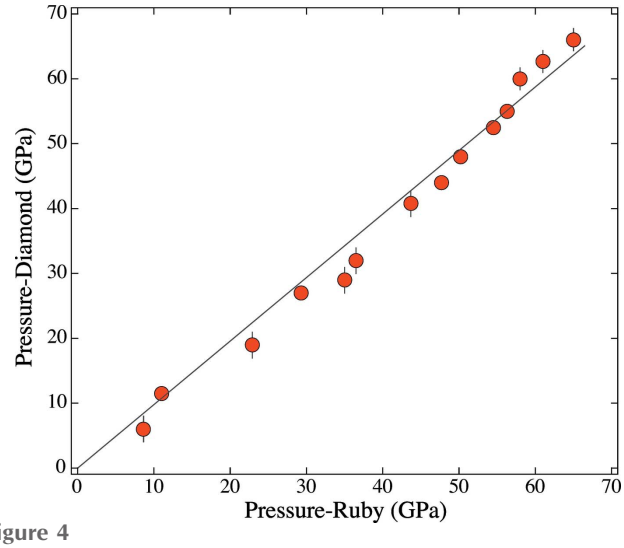

Figure 4
Pressure measured using two methods during decompression of a SiO_2 sample in miniature diamond anvils without recesses. The pressure (in GPa) given by the ruby fluorescence is reported on the horizontal axis, whereas the pressure measured on the tip of the diamond is reported on the vertical axis.

total diameter is reduced to less than one-third, from 3.1 mm down to 1 mm diameter. The thickness is reduced from 1.6 mm as in standard design down to 0.48 mm for the smallest anvils (Fig. 2*b*). The calculated X-ray transmission of 67% at 9.7 keV through one small anvil of 0.48 mm is nearly equivalent to the 76% transmission through 2.5 mm of beryllium (thickness of half of a standard Be gasket) (Fig. 3). Compared with standard anvils of 1.6 mm thickness, with a transmission of 25% at 9.7 keV (Fig. 3), the miniature anvils are three times less absorbent at 9.7 keV. All designs, without recess, have been tested with the same SiO_2 glass sample confined in a conventional rhenium gasket of 250 µm initial thickness and could reach pressures between 65 and 70 GPa measured by ruby fluorescence (Mao *et al.*, 1986) and by the Raman signal of the diamond culet (Akahama & Kawamura, 2006) (Fig. 4). All diamonds were recovered intact and can also be gas-loaded in a similar way to those of standard diamond anvils.

3.2. Milling recess in miniature diamond anvils

In order to further increase the sample-to-background ratio, it is essential to increase the path length of the sample exposed to the X-ray beam relative to the one of the diamond anvils. To reach a larger path length, or volume, for the sample, the culet of each diamond anvil was milled using the Scios DualBeam [focus-ion beam (FIB)] system (FEI Deutschland GmbH) at the Bayerisches Geoinstitut (BGI). Milling out a recess of between 15 and 20 µm depth (Figs. 5*a* and 5*b*) and 90–110 µm in diameter is obtained using a 50 nA beam with an acceleration voltage of 30 kV within 5 to 6 h. The milling procedure consisted of a succession of ten cylindrical patterns of 2 µm depth each with an incremental increase in diameter of 2 µm for each new cylinder. The first milling pattern was a 90 µm-diameter cylinder of 2 µm depth, followed by a 92 µm × 2 µm cylinder until the final step with a 110 µm × 2 µm cylinder. The double recess created an additional sample length along the beam of about 30 to 40 µm. Thus, the final thickness of the recovered SiO_2 glass sample, measured in the present study, was 50 µm after compression to a pressure of 60 GPa. This is

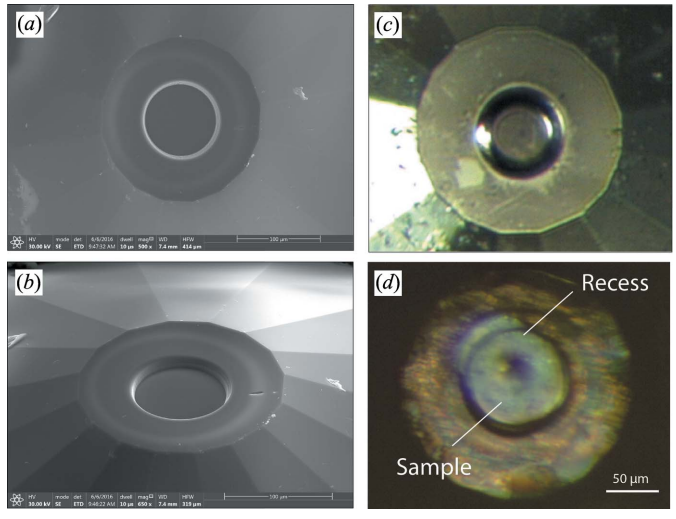

Figure 5
Recess manufacturing in the diamond anvil and loading. (*a*) and (*b*) Secondary electron images of a recess milled in the diamond culet using the Ga-ion gun of the Scios DualBeam at the BGI. The recess is ~17 µm deep and 100 µm in diameter. (*c*) Optical image of a diamond with a recess milled by the FIB. One can see that the optical transparency of the diamond is preserved in the recess. (*d*) Optical image of SiO_2 glass compressed in a rhenium gasket at 60 GPa between two milled-miniature diamonds.

three times thicker than the 17 μm thickness measured on a normal rhenium gasket recovered from a run with standard diamonds and pressurized to a similar pressure. The FIB milling also preserves the surface and the optical quality of the initial surface, keeping the diamond culet at the bottom of the recess optically transparent (Fig. 5*c*). This enables the use of lasers for measuring the ruby-fluorescence shift with pressure or Raman spectra of the diamond culet. This type of milling would also be very useful for laser heating or measuring Brillouin scattering for which a volume increase can serve to better insulate the sample or to increase the signal-to-background ratio at high pressure, respectively. The double recess also stabilizes the shape of the sample chamber and the gasket. The metallic rhenium gasket is pinched at the rim of the recess reducing the extrusion of gasket material toward the edges of the anvils (Boehler & De Hantsetters, 2004).

The larger sample volume created by the two recesses milled in both diamonds resulted in an increase of the applied force on the diamond to reach similar pressure conditions. This excess in the applied force created an over-pressure at the base of the diamond at the interface with the tungsten carbide (WC) seat. During our tests, we achieve a maximum pressure of 63 GPa with miniature anvils combined with WC seats. At such pressure the seats started to crumble, limiting our measurements for the smallest tested designs with 0.7 mm and 0.48 mm thickness. We did not observe such phenomena for the 0.9 mm diamond, as the surface contact with the WC seat was probably still large enough to distribute the pressure evenly at the interface. Polycrystalline diamond (Boehler *et al.*, 2013) or harder WC should be employed as support material for the miniature diamonds to sustain higher pressures. However, they are difficult to machine with such small dimensions.

4. XRS at the Si *L*-edge and O *K*-edge on SiO_2 glass at high pressure

To test our new miniature anvils and their capabilities for measuring low-energy absorption edges, we collected XRS spectra at the Si *L*-edge and O *K*-edge of SiO_2 glass at high pressures up to 47 GPa. Spectra on the starting glass, as well as on a quartz powder and on a stishovite polycrystalline sample, were measured as references of a fourfold and a sixfold coordinated structure, respectively. The collection time for each standard sample, covering both edges, was about 2 h. The sample was a suprasil-type SiO_2 glass finely ground into a powder. A 250 μm-thick rhenium foil was pre-indented down to 80 μm in between two miniature diamond anvils of 250 and 200 μm culet, both milled with ∼15–20 μm depth and 110 μm-diameter recesses, and was used as a gasket. A hole of 125 μm, slightly larger than the diameter of the recess, was drilled and served as the sample chamber for the SiO_2 powder. A ruby chip was placed 30 μm away from the centre in the powdered sample and used as a pressure gauge by following the shift of the ruby R1 line with pressure (Mao *et al.*, 1986). The XRS acquisition time at high pressure was less than six hours, for both edges, increasing the number of pressure points that can be measured during the short period of a synchrotron experiment.

4.1. O *K*-edge

Fig. 6 shows the results at the O *K*-edge for reference samples (glass and stishovite) at ambient conditions and the SiO_2 glass sample compressed to 18 and 47 GPa. Up to 18 GPa, a single asymmetric peak with a maximum at 539 eV, such as the one observed in the glass at room pressure, persists without showing sizable changes with increasing pressure. At high pressure, we can observe a broad doublet peak, having one shoulder at 539 eV and a second shoulder at 543 eV. This feature is very similar to the one measured for the stishovite reference at the O *K*-edge.

4.2. Si *L*-edge

Fig. 7 shows Si *L*-edge spectra obtained from the two reference samples, glass and stishovite, measured at room conditions as well as spectra from two measurements on the SiO_2 glass at 18 and 47 GPa. The doublet peak, observed on the glass at room pressure, is still observable at 18 GPa with, however, a change in the weight of the peak intensities. At even higher pressure a change in the structure occurs between 18 and 47 GPa, with the merging of the doublet peak into a single sharp peak, similar to the spectrum of the stishovite standard at room pressure with, however, a significant shift of the peak to higher energy loss. This provides clear evidence of

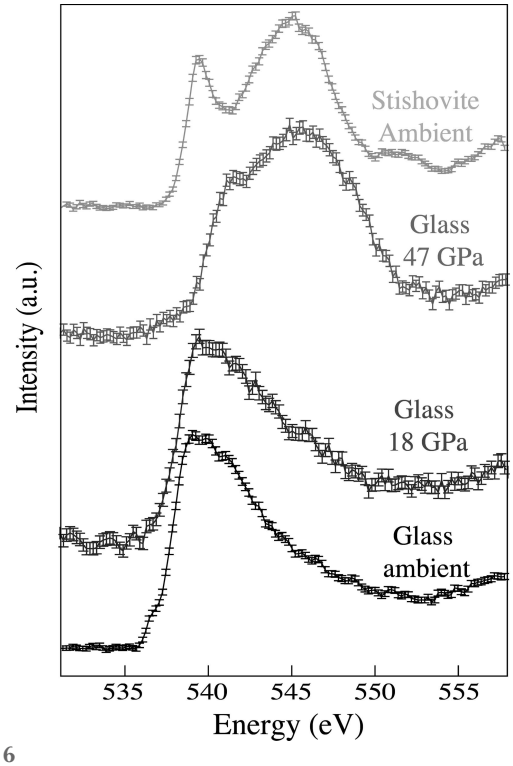

Figure 6
Spectra for the O *K*-edge collected on reference materials (glass and stishovite) at ambient conditions compared with those for the SiO_2 glass sample compressed at 18 and 47 GPa. The scattering vector for the measurements was q = 1.7 Å^{-1}.

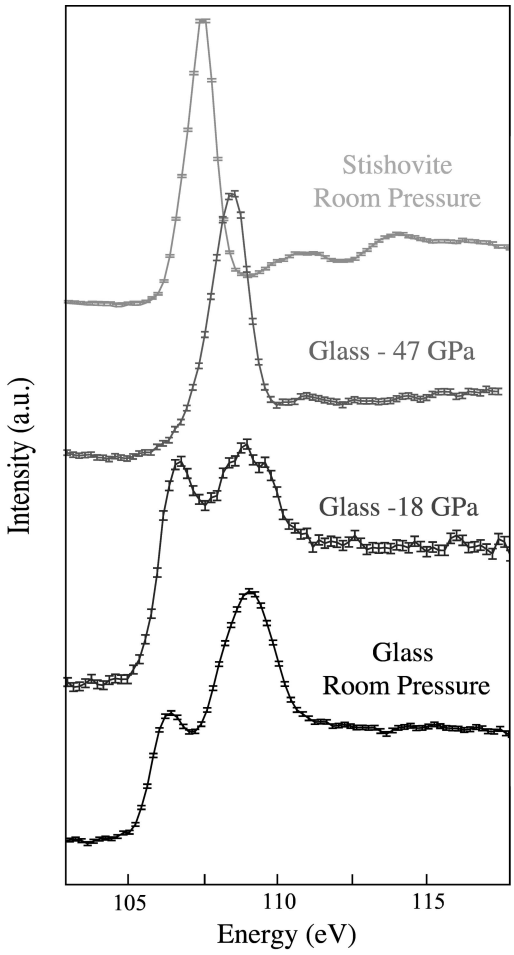

Figure 7
Spectra for the Si *L*-edge collected on reference materials (glass and stishovite) at ambient conditions compared with those for the SiO_2 glass sample compressed at 18 and 47 GPa. The scattering vector for the measurements was q = 1.7 Å^{-1}.

a change of coordination in SiO_2 glass from a fourfold coordinated structure to a higher, stishovite-like coordination number for Si at pressures above 20 GPa.

Based on the similarities between the Si *L*-edge and O *K*-edge spectra of the glass at high pressure and the reference samples, we can conclude that, up to 18 GPa, the SiO_2 glass preserves a fourfold coordination very similar to the one of the ambient conditions. At higher pressure, at least up to 47 GPa, a significant increase in coordination has occurred in the glass upon compression.

5. Conclusions

We have developed miniature diamond anvils that can sustain similar pressure conditions as the standard design with a similar culet size of 250 µm in diameter. The conical Boehler–Almax design of the miniature anvils allows for a high-angle scattering geometry with a 70° opening angle, essential to probe both low-q and high-q inelastic scattering signals from the sample under high pressure. The reduction of diamond thickness down to one-third of the classic design lowers the attenuation of the incoming X-ray beam as well as the one of the outgoing signal from the sample. The use of a FIB to mill out recesses of about 20 µm depth in the culet of each diamond anvil has increased the sample volume by a factor of three, significantly improving the signal-to-background ratio for XRS. The possibility of increasing the sample volume at high pressure, while keeping the transparency of the diamond to many optical probes, also opens up new perspectives to improve the signal quality when performing single-crystal XRD or Brillouin scattering, for which the sample volume is a critical parameter for the quality and accuracy of the measurements.

Our measurements on SiO_2 glass at high pressure confirm that a fourfold coordination is preserved up to 18 GPa. The coordination increases above 18 GPa, such that at 47 GPa both the O *K*-edge and the Si *L*-edge spectra resemble the one for stishovite with a sixfold silicon coordination. Our measurements are in contrast with previous reports where no indication of changes in the Si *L*-edge at high pressure was reported (Fukui *et al.*, 2008). However, the same changes are observed during the amorphization of α-quartz under similar pressure conditions (Sahle *et al.*, 2017). More data and molecular dynamic simulations are required to elucidate whether this spectral change represents a sixfold coordination, or a mixture of fivefold and sixfold and at which pressure the sixfold coordination could be completed.

The use of miniature diamond anvils offers new opportunities for high-pressure studies with techniques bound to X-ray energies strongly affected by attenuation in diamond (XANES, Mössbauer spectroscopy *etc.*). Our future work will focus on the combination of miniature diamonds with such X-ray techniques, as well as the use of laser heating. Further thickness reduction by 20 to 30% as well as higher pressure generation up to 100–120 GPa are also foreseen; thereby extending the capabilities and type of measurements of X-ray Raman scattering and other spectroscopic experiments at high pressure.

Acknowledgements

We acknowledge the ESRF for provision of beam time under the proposal ES-431. We acknowledge N. Dubrovinskaia for providing us with the stishovite standard material. SP is financed by a DFG grant (PE 2334/1-1). SP is particularly grateful to Almax-easylab company for the manufacturing of the miniature diamond anvils. The Scios Focus Ion Beam at BGI was financed by DFG grant No. INST 91/315-1 FUGG. CS and CW would like to thank M. Tolan for supporting these activities and acknowledge funding by the BMBF (05K13PE2 and 05K16PE1).

References

Akahama, Y. & Kawamura, H. (2006). *J. Appl. Phys.* **100**, 043516.
Benmore, C. J., Soignard, E., Amin, S. M., Guthrie, M., Shastri, S. D., Lee, P. L. & Yarger, J. L. (2010). *Phys. Rev. B*, **81**, 054105.
Bergmann, U., Glatzel, P. & Cramer, S. P. (2002). *Microchem. J.* **71**, 221–230.
Boehler, R. & De Hantsetters, K. (2004). *High Pressure Res.* **24**, 391–396.

Boehler, R., Guthrie, M., Molaison, J. J., dos Santos, A. M., Sinogeikin, S., Machida, S., Pradhan, N. & Tulk, C. A. (2013). *High Pressure Res.* **33**, 546–554.
Fister, T. T., Seidler, G. T., Shirley, E. L., Vila, F. D., Rehr, J. J., Nagle, K. P., Linehan, J. C. & Cross, J. O. (2008). *J. Chem. Phys.* **129**, 044702.
Fukui, H., Kanzaki, M., Hiraoka, N. & Cai, Y. Q. (2008). *Phys. Rev. B*, **78**, 012203.
Ghosh, D. B., Karki, B. & Stixrude, L. (2014). *Am. Mineral.* **99**, 1304–1314.
Hemley, R. J., Mao, H. K., Bell, P. M. & Mysen, B. O. (1986). *Phys. Rev. Lett.* **57**, 747–750.
Hiraoka, N., Fukui, H. & Okuchi, T. (2016). *High Pressure Res.* **36**, 250–261.
Hiraoka, N., Fukui, H., Tanida, H., Toyokawa, H., Cai, Y. Q. & Tsuei, K. D. (2013). *J. Synchrotron Rad.* **20**, 266–271.
Huotari, S., Pylkkänen, T., Verbeni, R., Monaco, G. & Hämäläinen, K. (2010). *Nat. Mater.* **10**, 489–493.
Krisch, M. & Sette, F. (2002). *Surf. Rev. Lett.* **09**, 969–976.
Lee, S. K., Eng, P. J. & Mao, H. (2014). *Rev. Mineral. Geochem.* **78**, 139–174.
Lee, S. K. *et al*. (2008). *Proc. Natl Acad. Sci. USA*, **105**, 7925–7929.
Lin, J.-F., Fukui, H., Prendergast, D., Okuchi, T., Cai, Y. Q., Hiraoka, N., Yoo, C.-S., Trave, A., Eng, P., Hu, M. Y. & Chow, P. (2007). *Phys. Rev. B*, **75**, 012201.
Mao, H. K., Xu, J. & Bell, P. M. (1986). *J. Geophys. Res.* **91**, 4673–4676.
Millot, M., Dubrovinskaia, N., Černok, A., Blaha, S., Dubrovinsky, L., Braun, D. G., Celliers, P. M., Collins, G. W., Eggert, J. H. & Jeanloz, R. (2015). *Science*, **347**, 418–420.
Mizuno, Y. & Ohmura, Y. (1967). *J. Phys. Soc. Jpn*, **22**, 445–449.
Mozzi, R. L. & Warren, B. E. (1969). *J. Appl. Cryst.* **2**, 164–172.
Murakami, M. & Bass, J. D. (2010). *Phys. Rev. Lett.* **104**, 025504.
Murakami, M. & Bass, J. D. (2011). *Proc. Natl Acad. Sci. USA*, **108**, 17286–17289.
Nilsson, A. D., Nordlund, I., Waluyo, N., Huang, H., Ogasawara, S., Kaya, U., Bergmann, U., Näslund, L.-Å., Öström, H., Wernet, P., Andersson, K. J., Schiros, T. & Pettersson, L. G. M. (2010). *J. Electron Spectrosc. Relat. Phenom.* **177**, 99–129.
Petitgirard, S., Malfait, W. J., Sinmyo, R., Kupenko, I., Hennet, K., Harries, D., Dane, T., Burghammer, M. & Rubie, D. C. (2015). *Proc. Natl Acad. Sci. USA*, **112**, 14186–14190.
Ponchut, C., Rigal, J. M., Clément, J., Papillon, E., Homs, A. & Petitdemange, S. (2011). *J. Instrum.* **6**, C01069.
Rueff, J.-P. & Shukla, A. (2010). *Rev. Mod. Phys.* **82**, 847–896.
Sahle, Ch. J., Mirone, A., Niskanen, J., Inkinen, J., Krisch, M. & Huotari, S. (2015). *J. Synchrotron Rad.* **22**, 400–409.
Sahle, Ch. J., Rosa, A. D., Rossi, M., Cerantola, V., Spiekermann, G., Petitgirard, S., Jacobs, J., Huotari, S., Moretti Sala, M. & Mirone, A. (2017). *J. Synchrotron Rad.* **24**, 269–275.
Sakamaki, T., Kono, Y., Wang, Y., Park, C., Yu, T., Jing, Z. & Shen, G. (2014). *Earth Planet. Sci. Lett.* **391**, 288–295.
Sanchez-Valle, C. & Bass, J. D. (2010). *Earth Planet. Sci. Lett.* **295**, 523–530.
Sanloup, C., Drewitt, J. W. E., Konôpková, Z., Dalladay-Simpson, P., Morton, D. M., Rai, N., van Westrenen, W. & Morgenroth, W. (2013). *Nature (London)*, **503**, 104–107.
Sato, T. & Funamori, N. (2008). *Phys. Rev. Lett.* **101**, 255502.
Schülke, W. (2007). *Electron Dynamics by Inelastic X-ray Scattering*. Oxford: Oxford Science Publications.
Sternemann, C., Soininen, J. A., Huotari, S., Vankó, G., Volmer, M., Secco, R. A., Tse, J. S. & Tolan, M. (2005). *Phys. Rev. B*, **72**, 035104.
Sternemann, C. & Wilke, M. (2016). *High Pressure Res.* **36**, 275–292.
Stixrude, L. & Karki, B. (2005). *Science*, **310**, 297–299.
Wernet, P., Nordlund, D., Bergmann, U., Cavalleri, M., Odelius, M., Ogasawara, H., Näslund, L. Å., Hirsch, T. K., Ojamäe, L., Glatzel, P., Pettersson, L. G. M. & Nilsson, A. (2002). *Science*, **304**, 995–999.
Woodcock, L. V., Angell, C. A. & Cheesman, P. (1976). *J. Chem. Phys.* **65**, 1565–1577.
Wu, M., Liang, Y., Jiang, J.-Z. & Tse, J. S. (2012). *Sci. Rep.* **2**, 398.
Yi, Y. S. & Lee, S. K. (2016). *Phys. Rev. B*, **94**, 094110.